

Disorder-mediated electron valley resonance in carbon nanotube quantum dots

András Pályi^{1,2} and Guido Burkard¹

¹Department of Physics, University of Konstanz, D-78457 Konstanz, Germany

²Department of Materials Physics, Eötvös University Budapest, H-1517 Budapest POB 32, Hungary

(Dated: February 24, 2024)

We propose a scheme for coherent rotation of the valley isospin of a single electron confined in a carbon nanotube quantum dot. The scheme exploits the ubiquitous atomic disorder of the nanotube crystal lattice, which induces time-dependent valley mixing as the confined electron is pushed back and forth along the nanotube axis by an applied ac electric field. Using experimentally determined values for the disorder strength we estimate that valley Rabi oscillations with a period on the nanosecond timescale are feasible. The valley resonance effect can be detected in the electric current through a double quantum dot in the single-electron transport regime.

PACS numbers: 76.20.+q, 73.63.Kv, 73.63.Fg, 71.70.Ej

Introduction. The conduction and valence bands of graphene and carbon nanotubes (CNTs) form two valleys as the bands approach each other at two non-equivalent points (K and K') of the Brillouin zone [1]. This twofold degeneracy of the electronic spectrum implies that the valley degree of freedom of an electron can be regarded as one bit of classical or quantum information, in analogy with the electron spin [2]. To evaluate the potential of encoding information in the valley degree of freedom, it is necessary to explore the physical mechanisms which could provide control over the valley state, as well as those leading to the loss of information.

Recent theoretical proposals suggest the use of valley-polarized edge states of zigzag graphene nanoribbons in a valley filter device [2], and non-adiabatic magnetic field sweeps for manipulation of the valley state of a single electron in a graphene Aharonov-Bohm ring [3]. However, the uncontrolled and strong valley mixing due to edge irregularities of nanostructured graphene might pose a significant challenge towards the realization of these ideas. This difficulty motivates the study of valley physics in CNTs, which have a rolled-up and therefore edge-free geometry. In fact, high-quality CNT quantum dots (QDs) have been fabricated recently [4–6] and the fourfold (spin and valley) quasi-degeneracy of the QD energy levels as well as very weak disorder have been experimentally confirmed [4, 5]. These ultraclean QD devices offer a chance for experimental realization of spin control via spin-orbit interaction [7] and manipulation of a combined spin-valley qubit (the “Kramers qubit”) utilizing a magnetic field, valley mixing, and bends in a CNT [8].

In this work we propose a scheme for coherent control of the valley isospin of a single electron, which is confined in a QD in a straight CNT at zero magnetic field. The effect, which we name *electron valley resonance* (EVR) in analogy to electron spin resonance (ESR), relies on short-range atomic disorder (substitutionals, adatoms, vacancies) of the CNT crystal lattice. Disorder induces harmonic time-dependent valley mixing as the confined electron is pushed back and forth along the CNT by an ap-

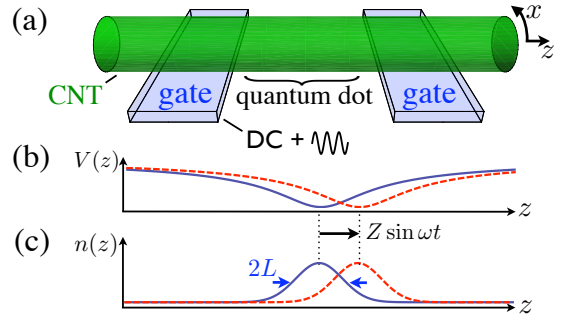


FIG. 1: (Color online) Schematic of the valley resonance setup. (a) Two gate electrodes close to the CNT confine an electron to the QD region. (b) The confinement potential $V(z)$ is periodically modulated in time by an ac voltage on the left gate. (c) The modulation of the confinement potential is followed by a displacement of the electron density $n(z)$. The interplay of this driven motion and the disorder on the CNT induces ac valley mixing leading to the valley resonance effect.

plied oscillating (ac) electric field (Fig. 1), which in turn induces Rabi oscillations between the two valley states. The ac electric field can be induced by applying an ac voltage component on one of the confining electrodes, as demonstrated in single-spin control experiments in GaAs QDs [9, 10].

Using a microscopic model [11, 12] of disorder-induced valley mixing, we map the valley dynamics of the oscillating electron to the two-level ESR problem. Together with a statistical treatment of possible disorder configurations, we find that the ratio between typical energy scales of the ac and static valley mixing is Z/L , where Z is the displacement amplitude of the electron and $2L$ is the width of the electronic wave function [see Eq. (4)]. As the static valley-mixing energy is measurable [4, 5], our finding can be used to estimate the ac component and hence the frequency of the valley Rabi oscillations. For a numerical example (see below) using data from [4], with $Z = 2$ nm and $L = 50$ nm we find that the time needed for a half Rabi oscillation between the two valley

states is ≈ 1.6 ns. We also describe a setup that could be used to detect the EVR effect via a measurement of the electric current in the regime of single-electron transport through a CNT double QD (DQD).

Microscopic theory of EVR. To model the electronic states we use the envelope function approximation and take the coordinates defined in Fig. 1. The Hamiltonian includes four terms: (i) the kinetic energy [11] $H_{\text{kin}} = v_F(\tau_3\sigma_1p_x + \sigma_2p_z)$ with Fermi velocity v_F , circumferential (longitudinal) electron momentum p_x (p_z), and σ_i (τ_i) being Pauli matrices acting in sublattice (valley) space; (ii) curvature-enhanced spin-orbit interaction [4, 13–15] $H_{\text{so}} = \tau_3s_z(\Delta_0 + \sigma_1\Delta_1)$ with axial spin component s_z and chirality-dependent on-site (off-site) spin-orbit matrix element Δ_0 (Δ_1); (iii) QD confinement potential $V_0(z)$, and (iv) disorder induced by atomic defects [11] which randomize the on-site energies on the crystal lattice,

$$H_{\text{dis}}(\mathbf{r}) = \Omega_{\text{cell}} \sum_l \sum_{\sigma=A,B} \sigma_\sigma [\tau_0 + \tau_r(\varphi_{l\sigma})] U_{l\sigma} \delta(\mathbf{r} - \mathbf{r}_{l\sigma}), \quad (1)$$

where $U_{l\sigma}$ is the on-site energy on site $\sigma \in (A, B) \equiv (+, -)$ in unit cell l . Here Ω_{cell} is the area of the unit cell of the graphene lattice, $\sigma_{A,B} = (\sigma_0 \pm \sigma_3)/2$, $\tau_r(\varphi) = \cos\varphi\tau_1 + \sin\varphi\tau_2$, $\varphi_{l\sigma} = \sigma(2\mathbf{K} \cdot \mathbf{r}_{l\sigma} - \eta) + \delta_{\sigma,B}2\pi/3$, η is the chiral angle of the CNT, $\mathbf{r}_{l\sigma}$ is the position of the lattice site $l\sigma$, and \mathbf{K} is the vector pointing to the K point of the Brillouin zone. The presence of the off-diagonal valley operator τ_r in H_{dis} reflects the fact that atomic disorder, due to its short-range character, allows for large momentum transfer upon scattering, including intervalley ($K \leftrightarrow K'$) transitions. Our valley rotation scheme relies on this K-K' coupling.

EVR is induced by pushing the confined electron back and forth along the z axis by applying an ac voltage on one of the gates (Fig. 1). We model this time-dependent displacement with the confinement potential $V(z, t) = V_0(z - Z \sin\omega t)$ with the ac frequency $\omega/2\pi$. To map the system to a two-level ESR problem, we first transform the complete Hamiltonian into the reference frame co-moving with the displaced electron. Thus we perform the time-dependent unitary transformation $U(t) = e^{iZ \sin(\omega t)p_z/\hbar}$, which leaves the position-independent kinetic energy and spin-orbit Hamiltonians H_{kin} and H_{so} invariant, but renders the confinement potential time-independent $V(z, t) \mapsto V_0(z)$ and the disorder term time-dependent $H_{\text{dis}}(\mathbf{r}) \mapsto H_{\text{dis}}(x, z + Z \sin\omega t)$. The additional term $i\hbar\dot{U}(t)U^{-1}(t)$, arising from the time-dependence of the transformation, can be neglected as it does not induce transitions within the ground state QD level.

As the next step, we restrict our consideration to the fourfold-degenerate (spin and valley) QD ground-state. For our purposes we can estimate the corresponding eigenfunctions of $H_{\text{kin}} + V_0(z)$ as Gaussians, having equal

weight on the two sublattices: $\Psi_{K,s}(x, z) \equiv |K\rangle\chi_s = \frac{e^{iqx}}{\sqrt{2\pi R}}(G_L(z), G_L(z), 0, 0)\chi_s$, and $\Psi_{K',s}(x, z) \equiv |K'\rangle\chi_s = \frac{e^{-iqx}}{\sqrt{2\pi R}}(0, 0, G_L(z), G_L(z))\chi_s$, with spinors χ_s having spin projection $s \in (\uparrow, \downarrow) \equiv (+, -)$ along the z axis, circumferential wave number $q > 0$, CNT radius R , and $G_L(z) = \frac{e^{-z^2/2L^2}}{\pi^{1/4}\sqrt{2L}}$. Projecting the spin-orbit Hamiltonian to this four-fold degenerate subspace yields $\bar{H}_{\text{so}} = \frac{1}{2}\Delta_{\text{SO}}s_z(|K'\rangle\langle K'| - |K\rangle\langle K|)$, where $\Delta_{\text{SO}} = 2(\Delta_0 + \Delta_1)$; experimentally reported values [4, 5, 16] of Δ_{SO} are in the range 0.17–2.5 meV. The form of \bar{H}_{so} implies that spin-orbit interaction induces an energy splitting Δ_{SO} between two valley states having the same spin direction. Therefore, as in the case of ESR in CNT QDs [7], no magnetic field is needed for EVR. Henceforth we restrict our considerations to the limit of small displacements $Z/L \ll 1$. By projecting the disorder Hamiltonian to the four-dimensional subspace of interest we find

$$\bar{H}_{\text{dis}} = (be^{i\phi} + b_{\text{ac}}e^{i\phi_{\text{ac}}} \sin\omega t)|K'\rangle\langle K| + \text{h.c.}, \quad (2)$$

where valley-diagonal terms are omitted. The real quantities b , ϕ , b_{ac} and ϕ_{ac} describe disorder-induced static and ac valley mixing and can be expressed in terms of $U_{l\sigma}$ and $\Psi_{v,s}$. Randomness of the disorder configuration $U_{l\sigma}$ implies the randomness of those quantities as well. Assuming a homogeneous and uncorrelated distribution of the atomic defects $\langle U_{l\sigma}U_{l'\sigma'} \rangle = \langle U_{l\sigma}^2 \rangle \delta_{l\sigma, l'\sigma'}$, with zero average $\langle U_{l\sigma} \rangle = 0$, we find $\langle b \rangle = \langle b_{\text{ac}} \rangle = 0$ and

$$\langle b^2 \rangle = \frac{1}{4\sqrt{2}\pi^{3/2}} \frac{\Omega_{\text{cell}}}{RL} \langle U_{l\sigma}^2 \rangle, \quad (3)$$

$$\langle b_{\text{ac}}^2 \rangle = \left(\frac{Z}{L}\right)^2 \langle b^2 \rangle. \quad (4)$$

Equations (2) and (4) are the central results of this work. The ac valley-mixing term $\propto b_{\text{ac}}$ in Eq. (2), induced by the simultaneous presence of the ac electric field and atomic disorder, allows for coherent rotations of the valley isospin similarly to a transverse magnetic field in ESR [21]. Furthermore, using the remarkably simple expression in Eq. (4) we can estimate the corresponding Rabi frequency from a measurement of the static valley-mixing element b . For example, in [4] a spin-orbit splitting of $\Delta_{\text{SO}} = 370 \mu\text{eV}$ and a valley gap of $\Delta_{KK'} = 65 \mu\text{eV}$ was found. Identifying $\Delta_{KK'}$ with $2\sqrt{\langle b^2 \rangle}$, and taking $L = 50$ nm and $Z = 2$ nm, from Eq. (4) we find an estimate for the strength of the ac valley-mixing term in this sample as $\sqrt{\langle b_{\text{ac}}^2 \rangle} = 1.3 \mu\text{eV}$. This value translates to a $\pi\hbar/\sqrt{\langle b_{\text{ac}}^2 \rangle} \approx 1.6$ ns long half Rabi cycle between two orthogonal valley states at resonant driving $\hbar\omega = \sqrt{\Delta_{\text{SO}}^2 + 4b^2}$.

Detection. We now describe a setup where EVR could be detected (Fig. 2). A serially coupled DQD between a source and a drain lead is tuned appropriately (see below for details), such that during the single-electron transport

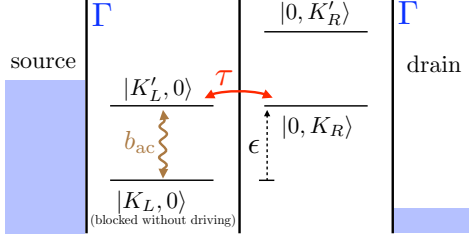


FIG. 2: (Color online) Schematic of EVR detection. The disorder-mediated ac valley mixing drives transitions between the states on the left QD. Interdot tunneling between K'_L and K_R has the amplitude $\tau e^{i\phi_\tau} = t\langle K_R|K'_L\rangle$.

process the electron can be trapped in a specific valley state in the left QD. ($|K_L, 0\rangle$ in Fig. 2). The valley state of a trapped electron is changed due to the EVR mechanism when an ac electric field is applied to the left QD. This allows the particle to exit via the ground state level of the right QD, thus EVR is detected via the measurement of the electric current through the DQD. Since this method is based on single-electron transport, it is unaffected by strong correlations, unlike the Pauli blockade effect [5, 12, 17, 18].

To describe the transport process outlined above, from now on we consider only spin- \uparrow electrons; hence the spin-orbit Hamiltonian simplifies to $\bar{H}_{\text{so}} = \frac{1}{2}\Delta_{\text{SO}}(|K'\rangle\langle K'| - |K\rangle\langle K|)$. The description of the spin- \downarrow electrons is completely analogous. As shown in Fig. 2, the energy levels in the DQD are tuned by gate electrodes so that the higher-lying sublevel in the left QD is aligned with the lower-lying sublevel in the right QD. We consider single-electron transport via the $(0, 0) \rightarrow (1, 0) \rightarrow (0, 1) \rightarrow (0, 0)$ transport cycle where (n, m) refers to the charge configuration with n (m) electrons in the left (right) QD. Interdot tunneling is assumed to be spin- and valley-conserving, therefore the static Hamiltonian of a single electron in the DQD is

$$H_{\text{DQD}} = \begin{pmatrix} -\frac{\Delta_{\text{SO}}}{2} & b_L e^{-i\phi_L} & t & 0 \\ b_L e^{i\phi_L} & \frac{\Delta_{\text{SO}}}{2} & 0 & t \\ t & 0 & -\frac{\Delta_{\text{SO}}}{2} + \epsilon & b_R e^{-i\phi_R} \\ 0 & t & b_R e^{i\phi_R} & \frac{\Delta_{\text{SO}}}{2} + \epsilon \end{pmatrix}, \quad (5)$$

where we use the basis $|K, 0\rangle, |K', 0\rangle, |0, K\rangle, |0, K'\rangle$, and $L, R = 0, K, K'$ in $|L, R\rangle$ refer to the occupation and valley state in the left and right QDs. The left-right energy detuning, needed for the level alignment described above, is $\epsilon = (\sqrt{\Delta_{\text{SO}}^2 + 4b_L^2} + \sqrt{\Delta_{\text{SO}}^2 + 4b_R^2})/2$. For the sake of simplicity and clarity, from now on we assume $b_{L,R} \ll \Delta_{\text{SO}}$ (as found in recent experiments [4, 5]), and $t \ll \Delta_{\text{SO}}$ (tunability of the interdot tunneling has been demonstrated in CNT DQDs [19]). A crucial point for our detection scheme is that the electron interacts with a different set of impurities in the two different QDs, and therefore b_L and ϕ_L are in general different from b_R and

ϕ_R . Together with the condition $b_{L,R} \ll \Delta_{\text{SO}}$, this implies that the higher-lying energy eigenstate in the left QD $|K'_L\rangle$ has a small K component, the lower-lying state in the right QD $|K_R\rangle$ has a small K' component, and $|K'_L\rangle$ is typically not orthogonal to $|K_R\rangle$. This leads to a finite tunneling matrix element $\tau e^{i\phi_\tau} = t\langle K_R|K'_L\rangle$ between the two aligned levels $|K'_L, 0\rangle$ and $|0, K_R\rangle$. This nonzero matrix element is required for the EVR detection scheme we outline below.

The level structure shown in Fig. 2 results in a blockade effect in a finite source-drain voltage bias. If the incoming electron enters the QD in the higher-lying $|K'_L, 0\rangle$ state then it can move through the DQD easily because of the complete hybridization of $|K'_L, 0\rangle$ with $|0, K_R\rangle$. However, the condition $t \ll \Delta_{\text{SO}}$ ensures that hybridization of the lower-lying state $|K_L, 0\rangle$ with $(0, 1)$ states is small ($\lesssim t/\Delta_{\text{SO}}$ in amplitude); therefore an electron occupying that state blocks transport as it exits the DQD slowly. Assuming equal tunneling rates Γ at source and drain, from a transport model based on the secular approximation ($\Gamma \ll t, b_{L,R}, \Delta_{\text{SO}}$) of the Born-Markov master equation we estimate that the current through the DQD without ac driving is much smaller than barrier transparency Γ ,

$$I_0/e \approx 2\Gamma(t/\Delta_{\text{SO}})^2 \ll \Gamma. \quad (6)$$

This transport blockade allows for detection of the EVR effect described above. If an ac electric field is active in the left QD and pushes back and forth the electron within the left dot, occupying the blocking lower-lying state $|K_L, 0\rangle$ in Fig. 2, then it undergoes a Rabi transition to the higher-lying $|K'_L, 0\rangle$ state, which allows it to exit the DQD to the drain due to the strong hybridization of $|K'_L, 0\rangle$ and $|0, K_R\rangle$. This process is most effective around resonant driving, i.e., when $\hbar\omega \approx \sqrt{\Delta_{\text{SO}}^2 + 4b_L^2}$. In fact, below we show that around the resonance condition and an appropriate tuning of the tunneling amplitude τ the current through the DQD approaches its maximal value $2e\Gamma/7$.

To provide an analytical result for the ac-field-induced current we neglect perturbative hybridization amplitudes between $(1, 0)$ and $(0, 1)$ states which are $\lesssim t/\Delta_{\text{SO}}$. In this simplified picture the higher-lying level $|0, K'_R\rangle$ on the right QD is not involved in the transport problem as it is not hybridized with $(1, 0)$ states. After a transformation into the rotating frame in the left QD and the counter-rotating frame in the right QD, and within the rotating wave approximation (RWA), the dynamics in the remaining three-level system can be described by

$$H_{\text{RWA}} \approx \delta |K_L, 0\rangle\langle K_L, 0| + \left(\frac{b_{\text{ac}}}{2} |K'_L, 0\rangle\langle K_L, 0| + \tau |0, K_R\rangle\langle K'_L, 0| + \text{h.c.} \right) \quad (7)$$

with the ac valley-mixing term $\propto b_{\text{ac}}$ and the detuning parameter $\delta = \hbar\omega - \sqrt{\Delta_{\text{SO}}^2 + 4b_L^2}$. The phases ϕ_{ac} and

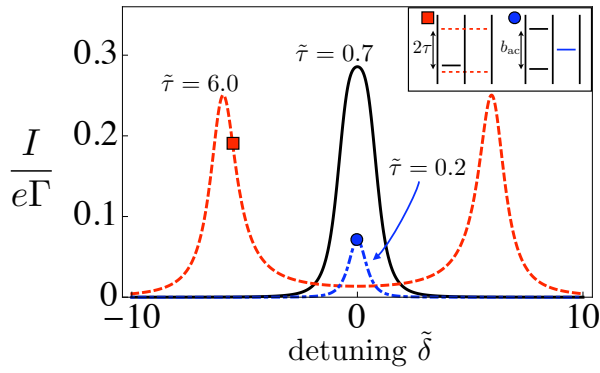


FIG. 3: (Color online) Current as function of the dimensionless detuning $\tilde{\delta} = \delta/b_{ac}$ of the driving frequency from resonance, for different values of the dimensionless tunneling amplitude $\tilde{\tau} = \tau/b_{ac}$. Inset: Energy diagrams corresponding to the two indicated points of the main plot.

ϕ_τ have been eliminated by a specific choice of the basis states. A small term $\propto b_{ac}b/\Delta_{SO}$ has been neglected in Eq. (7). The leading-order (in Γ) analytical result for the current, obtained from the Born-Markov master equation transport model is

$$\frac{I}{e\Gamma} = \frac{2\tau^2 b_{ac}^2}{4\tau^4 + \tau^2(3b_{ac}^2 - 8\delta^2) + 4\delta^4 + 5\delta^2 b_{ac}^2 + b_{ac}^4}. \quad (8)$$

Using Eq. (8), in Fig. 3 we plot the current as a function of dimensionless detuning $\tilde{\delta} = \delta/b_{ac}$ for three different values of the dimensionless tunneling amplitude $\tilde{\tau} = \tau/b_{ac}$. The three curves correspond to three different regimes: (i) For $\tilde{\tau} = 6.0$ the current shows two Lorentzian peaks as the function of detuning, which have width $b_{ac}/\sqrt{2}$ and maximal current $e\Gamma/4$ in the entire $\tilde{\tau} \gg 1$ regime. In this situation, hybridization of $|K'_L, 0\rangle$ and $|0, K_R\rangle$ results in a ‘bonding’ and an ‘antibonding’ state having energies $\mp\tau$, depicted as dashed lines in the left diagram of the inset of Fig. 3. The ac field can be resonant with only one of these states (in the inset it is the bonding one), as the current peak width is set by the Rabi energy b_{ac} , which is significantly smaller than the peak separation 2τ in this case. This parameter regime seems to be suitable for EVR detection as the resonant current is large, i.e., comparable to the tunneling rate of the lead-dot barriers (see, however, estimate of the background current I_0 below). (ii) For $\tilde{\tau} = 0.7$, the energy separation 2τ between the two peaks of regime (i) becomes comparable to the Rabi energy b_{ac} , and therefore the two peaks merge into a single one. This parameter setting is optimal for EVR detection as the peak value of the current is $2e\Gamma/7$, exceeding that in regime (i). (iii) For $\tilde{\tau} = 0.2$, the Rabi energy b_{ac} becomes dominant over interdot tunneling τ . This implies that the minimal energy distance between the two $(1,0)$ states cannot drop below b_{ac} , and current is maximal if they hybridize equally ($\propto \tau/b_{ac}$) with $|0, K_R\rangle$ (this maximal-current sit-

uation is shown in the right diagram of the inset of Fig. 3). This $\tilde{\tau} \ll 1$ regime is less suitable for EVR detection as the peak current is only a small fraction $2\tilde{\tau}^2\Gamma$ of the barrier transparency Γ . The line shape is approximately a Lorentzian for small detuning, with width $b_{ac}/\sqrt{5}$.

To take a numerical example, we use again $b_{ac} = 1.3 \mu\text{eV}$, $\Delta_{SO} = 370 \mu\text{eV}$, $b_L = b_R = 32.5 \mu\text{eV}$, $\phi_R - \phi_L = \pi/3$, which yields $\tau \approx 0.075t$. This implies that by tuning t to $90.2 \mu\text{eV}$, $10.5 \mu\text{eV}$ and $3.0 \mu\text{eV}$, one arrives to the previously plotted and described situations (i), (ii) and (iii), respectively. Furthermore, it is reasonable to assume a lead-dot tunneling rate $\Gamma = 62.5 \text{ MHz}$, which translates to a measurable current scale $e\Gamma \approx 10 \text{ pA}$, and a tunneling-induced level broadening of $\hbar\Gamma \approx 40 \text{ neV} \ll b_{ac}, \tau$ in all cases. We also estimate the EVR detection visibility by comparing the background current I_0 [see Eq. (6)], i.e., the current in the absence of the ac electric field, to the current at resonant EVR driving. In the cases (i), (ii) and (iii), the background current I_0 is estimated from Eq. (6) as 1.2 pA , 16 fA and 1 fA , respectively. For this numerical example, we can conclude that in cases (ii) and (iii) the background current is much smaller than the EVR contribution due to the ac electric field ($\sim 1 \text{ pA}$ from Fig. 3 and $e\Gamma = 10 \text{ pA}$), and therefore EVR could indeed be detected in this transport measurement.

Valley relaxation, e.g., mediated by valley mixing and accompanied by phonon emission, can affect the dynamics of the EVR. By including valley relaxation in our transport model, we have found that the results shown in Fig. 3 do not change significantly as long as the valley relaxation rate is below b_{ac}/\hbar and τ/\hbar . In principle, EVR could also be detected by generalizing the proposed setup to pulsed-gated transport or charge sensing experiments [5, 9, 10, 20], which may allow for measuring the valley decoherence time scale. Finally, we note that the ideas described in this paper in the context of CNTs could be generalized to QDs in other multivalley materials, such as silicon.

We acknowledge DFG for financial support within Grants No. SFB 767, SPP 1285, and FOR 912.

-
- [1] R. Saito, G. Dresselhaus, and M. Dresselhaus, *Physical Properties of Carbon Nanotubes* (Imperial College Press, 1998).
 - [2] A. Rycerz, J. Tworzydło, and C. W. J. Beenakker, *Nat. Phys.* **3**, 172 (2007).
 - [3] P. Recher, B. Trauzettel, A. Rycerz, Y. M. Blanter, C. W. J. Beenakker, and A. F. Morpurgo, *Phys. Rev. B* **76**, 235404 (2007).
 - [4] F. Kuemmeth, S. Ilani, D. C. Ralph, and P. L. McEuen, *Nature* **452**, 448 (2008).
 - [5] H. O. H. Churchill, F. Kuemmeth, J. W. Harlow, A. J. Bestwick, E. I. Rashba, K. Flensberg, C. H. Stwertka, T. Taychatanapat, S. K. Watson, and C. M. Marcus,

- Phys. Rev. Lett. **102**, 166802 (2009).
- [6] G. A. Steele, G. Gotz, and L. P. Kouwenhoven, Nat. Nanotechnol. **4**, 363 (2009).
 - [7] D. V. Bulaev, B. Trauzettel, and D. Loss, Phys. Rev. B **77**, 235301 (2008).
 - [8] K. Flensberg and C. M. Marcus, Phys. Rev. B **81**, 195418 (2010).
 - [9] K. C. Nowack, F. H. L. Koppens, Y. V. Nazarov, and L. M. K. Vandersypen, Science **318**, 1430 (2007).
 - [10] E. A. Laird, C. Barthel, E. I. Rashba, C. M. Marcus, M. P. Hanson, and A. C. Gossard, Phys. Rev. Lett. **99**, 246601 (2007).
 - [11] T. Ando and T. Nakanishi, J. Phys. Soc. Jpn. **67**, 1704 (1998).
 - [12] A. Pályi and G. Burkard, Phys. Rev. B **82**, 155424 (2010).
 - [13] T. Ando, J. Phys. Soc. Jpn. **69**, 1757 (2000).
 - [14] J.-S. Jeong and H.-W. Lee, Phys. Rev. B **80**, 075409 (2009).
 - [15] W. Izumida, K. Sato, and R. Saito, J. Phys. Soc. Jpn. **78**, 074707 (2009).
 - [16] S. H. Jhang, M. Marganska, Y. Skourski, D. Preusche, B. Witkamp, M. Grifoni, H. van der Zant, J. Wosnitzer, and C. Strunk, Phys. Rev. B **82**, 041404 (2010).
 - [17] H. O. H. Churchill, A. J. Bestwick, J. W. Harlow, F. Kuemmeth, D. Marcos, C. H. Stwertka, S. K. Watson, and C. M. Marcus, Nat. Phys. **5**, 321 (2009).
 - [18] A. Pályi and G. Burkard, Phys. Rev. B **80**, 201404(R) (2009).
 - [19] N. Mason, M. J. Biercuk, and C. M. Marcus, Science **303**, 655 (2004).
 - [20] F. H. L. Koppens, C. Buizert, K. J. Tielrooij, I. T. Vink, K. C. Nowack, T. Meunier, L. P. Kouwenhoven, and L. M. K. Vandersypen, Nature **442**, 766 (2006).
 - [21] Note that here the ac valley-mixing field is not strictly transversal to the static Hamiltonian if b is finite. However, if $b \ll \Delta_{\text{SO}}$, as found in recent experiments [4, 5], then the ac field is transversal to a good approximation.